International Journal of Chemical Science
www.chemicaljournals.com
Online ISSN: 2523-2843
Received: 01-05-2026, Accepted: 01-06-2026, Published: 16-06-2026
Volume 10, Issue 2, 2026, Page No. 89-94

Targeting CDK1 and CDK2 in cancer: From cell-cycle biology to selective inhibitor design, a computational perspective

Ganga Grazielia Chrisna, Chen Qu
Zhejiang University of Science and Technology, Hangzhou, Zhejiang, China
DOI: https://doi.org/10.66856/chemical.2026.10.2.10031

Abstract
Cyclin-dependent kinases 1 and 2 (CDK1 and CDK2) are essential regulators of the eukaryotic cell cycle and compelling oncology drug targets. Their near-identical ATP-binding pockets, sharing a global backbone RMSD of ~0.72 Å, present a fundamental selectivity challenge: inhibitors must discriminate between two kinases whose active sites are virtually superimposable. This review bridges the biological rationale for CDK targeting with computational evidence from 100 ns all-atom molecular dynamics simulations, global conformational stability analysis, and alchemical free energy calculations for five CDK–inhibitor complexes involving Dinaciclib, AZD5438, and CGP74514A. Radius of gyration (Rg) analysis confirms that both kinases maintain native globular-fold stability throughout the simulation (Rg = 1.92–2.06 nm), indicating that differences in selectivity are not driven by global structural destabilization. van der Waals decoupling profiles from AZD5438 alchemical simulations reveal a characteristic non-monotonic free-energy landscape with a peak of ~8.7 kT in the early λvdW windows, providing direct energetic evidence for the steric and dispersive contributions to CDK2 selectivity. Integrated with the cell-cycle biology of CDK/cyclin complexes and the pharmacological classification of kinase inhibitors (Types I–IV), these findings establish a multi-scale framework, from oncogenic signaling pathways to sub-Ångström pocket dynamics, for rational CDK2-selective drug design.

Keywords: CDK1, CDK2, cell cycle, kinase inhibitor, selectivity, molecular dynamics, alchemical free energy, radius of gyration, Van Der Waals decoupling, oncology

Introduction

Cancer is fundamentally a disease of dysregulated cell division, and the kinases that orchestrate the cell cycle occupy a central position in oncological drug discovery. Among these, cyclin-dependent kinases (CDKs) have attracted sustained therapeutic interest for over three decades [3]. CDKs are serine/threonine protein kinases that require association with regulatory cyclin subunits and phosphorylation by CDK-activating kinase (CAK) for catalytic activation. They govern the sequential transitions between cell-cycle phases, G1, S, G2, and M, through the phosphorylation of downstream effectors including the retinoblastoma protein (RB), E2F transcription factors, and lamins [4, 5].

The clinical success of CDK4/6 inhibitors, palbociclib, ribociclib, and abemaciclib, in hormone receptor-positive breast cancer has validated CDK inhibition as a precision oncology strategy and reinvigorated interest in targeting the broader CDK family [2, 3]. CDK1 and CDK2 are the most structurally similar members of this family and occupy distinct but overlapping regulatory niches: CDK2–Cyclin E and CDK2–Cyclin A drive the G1/S transition and initiation of DNA replication, while CDK1–Cyclin A and CDK1–Cyclin B are indispensable for mitotic entry and progression [6]. Crucially, CDK1 is the only essential CDK in mammals; it can compensate for the loss of other CDKs, making selective CDK2 inhibition the preferred therapeutic strategy to minimize mitotic toxicity [7].

The selectivity challenge is a crystallographic paradox. X-ray co-crystal structures of CDK1 and CDK2 with ATP-competitive inhibitors reveal near-superimposable binding pockets. Yet, experimental isothermal titration calorimetry (ITC) demonstrates that inhibitors such as AZD5438 achieve 170-fold CDK2 selectivity (Kd = 26 nM for CDK2 versus 4,400 nM for CDK1) [3]. This gap between static structural similarity and dynamic functional selectivity motivates computational investigation at multiple scales: from the oncogenic signaling cascades that make CDKs therapeutic targets, through the pharmacological classification of kinase inhibitors, to sub-nanosecond pocket dynamics and

structural basis for selectivity at each type. Third, we present original computational data, global conformational alchemical free-energy landscapes that quantify binding thermodynamics.

This review integrates three levels of analysis. First, we contextualize CDK1/CDK2 within the oncogenic signaling network and cell-cycle regulatory machinery that justify their therapeutic targeting. Second, we classify CDK inhibitors within the established kinase inhibitor taxonomy (Types I–IV) and highlight the stability from radius-of-gyration analysis, and van der Waals free-energy decoupling profiles from alchemical simulations of CDK1/CDK2–AZD5438, which provide mechanistic insight into the energetic origins of selectivity not accessible from crystallography alone. Together, these analyses establish a multi-scale framework linking cancer biology to atomic-level drug design.

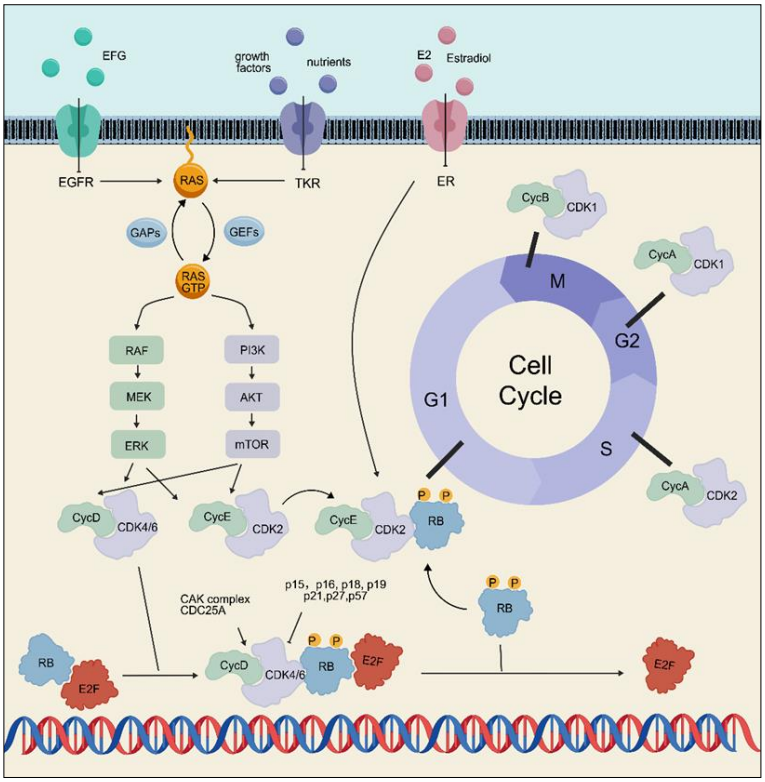

Fig 1: CDK/cyclin signaling pathways and cell-cycle phase regulation

CDK1 and CDK2 as Oncology Targets

1. Oncogenic Context and Therapeutic Rationale

CDK2 is hyperactivated in a broad spectrum of human cancers through multiple convergent mechanisms: amplification of cyclin E1 (CCNE1) in ovarian and gastric carcinomas, loss of the CDK inhibitor p27Kip1 in breast and colorectal cancers, and constitutive activation of upstream RAS/MAPK and PI3K/AKT signaling pathways that drive cyclin D and cyclin E transcription [3, 9]. CDK2 hyperactivation accelerates S-phase entry, promotes genomic instability through premature origin firing and replication stress, and enables tumor cells to bypass DNA damage checkpoints, making CDK2 a compelling target for both direct inhibition and synthetic lethality strategies [6].

CDK1, while essential for mitosis, is paradoxically an attractive target in specific contexts. Synthetic lethality between CDK1 inhibition and defects in DNA damage response pathways, particularly in BRCA1/2-mutant and RB-deficient tumors, suggests that CDK1 inhibitors may have a therapeutic window in genetically defined patient populations [11]. Moreover, triple-negative breast cancer (TNBC) and small-cell lung cancer (SCLC) display high mitotic indices and CDK1 dependency that may be exploited pharmacologically. The therapeutic challenge, however, remains selectivity: CDK1 is essential for normal cell division, and non-selective CDK1/CDK2 inhibitors cause severe hematological toxicity due to suppression of hematopoietic progenitor proliferation [12].

2. Structural Basis of CDK Homology and the Selectivity Problem

CDK1 and CDK2 share approximately 65% sequence identity and maintain essentially identical catalytic machinery. The ATP-binding cleft, bound by virtually all clinically relevant inhibitors, is delineated by the hinge region (connecting N- and C-terminal lobes), the glycine-rich P-loop, the αC-helix (containing the PSTAIRE motif in CDK2 and an equivalent PSTAVRE motif in CDK1), and the activation loop bearing the DFG motif [3]. Superposition of CDK1 and CDK2 crystal structures yields a global backbone RMSD of ~0.72 Å. The residues lining the ATP pocket differ at only a few positions, most notably Cys83 (CDK2) versus Thr85 (CDK1) and His84 (CDK2) versus Asp86 (CDK1), neither of which is directly contacted by all inhibitor scaffolds [7, 16].

This structural near-identity means that most competitive inhibitors bind both CDK1 and CDK2 with comparable affinities. The selectivity that does exist, as exemplified by AZD5438's 170-fold CDK2 preference, must therefore arise not from direct steric exclusion by differing residues but from subtler dynamic and thermodynamic differences: conformational flexibility of the binding pocket, ordering of interfacial water molecules, and the energetic costs of induced-fit rearrangements that differ between the two isoforms despite their structural similarity [1, 3].

Classification of Kinase Inhibitors

1. Type I and Type II Inhibitors: ATP-Competitive Binding

The pharmacological taxonomy of kinase inhibitors, originally proposed by Dar and Shokat and subsequently elaborated by numerous groups, provides a conceptual framework for understanding the structural basis of selectivity [4]. Type I inhibitors bind the active (DFG-in) conformation of the kinase, competing directly with ATP for occupancy of the hinge-binding region. They form hydrogen bonds with hinge backbone atoms and extend into the hydrophobic back pocket. Because the active conformation is highly conserved across the kinome, Type I inhibitors tend to exhibit lower selectivity. However, careful optimization of pocket-filling hydrophobic contacts can enhance selectivity within subfamilies [18].

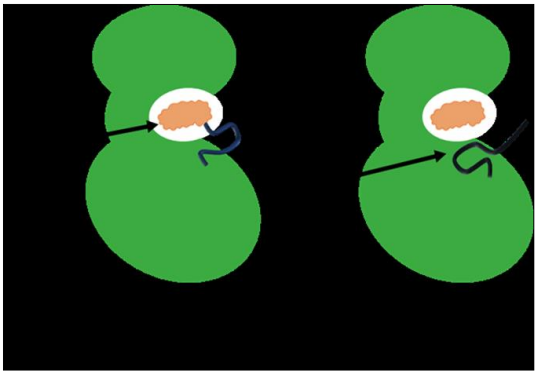

Fig 2: Type I and Type II kinase inhibitor binding modes

Type II inhibitors exploit the inactive DFG-out conformation, extending beyond the adenine-binding site into a hydrophobic allosteric pocket accessible only when the DFG motif flips outward. Because this inactive conformation is less conserved across kinases than the active conformation, Type II inhibitors generally achieve greater selectivity. The paradigm example is imatinib, which selectively inhibits ABL kinase in the DFG-out conformation, sparing most other kinases [19]. However, CDK1 and CDK2, being proline-directed kinases with a structurally constrained activation loop, have limited capacity to adopt the DFG-out conformation, thereby restricting CDK inhibitor development primarily to the Type I scaffold.

2. Type III and Type IV: Allosteric Inhibitors

Type III inhibitors bind within the ATP site but at an allosteric location immediately adjacent to the ATP-binding cleft (allosteric within the ATP site), relying on unique conformational features of a specific kinase to achieve selectivity. Type IV inhibitors bind at allosteric sites that are entirely remote from the ATP pocket, thereby achieving the highest degree of selectivity by exploiting unique structural elements of the target kinase that are not conserved across the kinome [20].

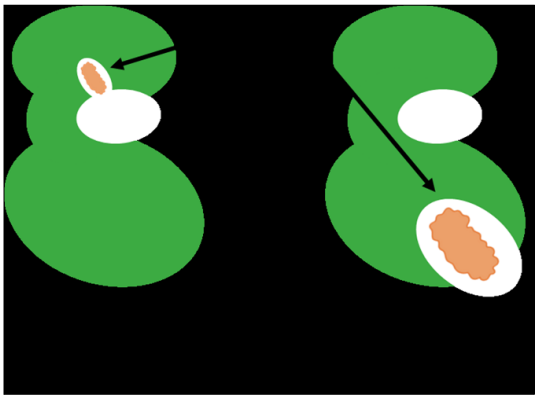

Fig 3: Type III and Type IV allosteric inhibitor binding modes

All three inhibitors studied computationally in this work, Dinaciclib, AZD5438, and CGP74514A, are Type I ATP-competitive inhibitors that bind the DFG-in conformation of CDK1 and CDK2. They form canonical hinge hydrogen bonds and extend into the hydrophobic back pocket. The selectivity differences between them arise solely from the quality and persistence of their interactions within this conserved binding mode, as quantified by molecular dynamics trajectory analysis and alchemical free-energy calculations.

Structural Diversity of CDK-Relevant Kinases

To contextualize CDK1/CDK2 selectivity within the broader kinase landscape, Figure 4 illustrates the three-dimensional structures of representative kinases from other oncologically relevant families. AKT1 (a serine/threonine kinase in the PI3K/mTOR pathway), ABL1 (the tyrosine kinase target of imatinib), and PI3Kα (a lipid kinase) share the two-lobe kinase fold but display pronounced structural divergence in their activation loops, αC-helices, and gate-keeper residues that underpin their pharmacological tractability with selective agents [1].

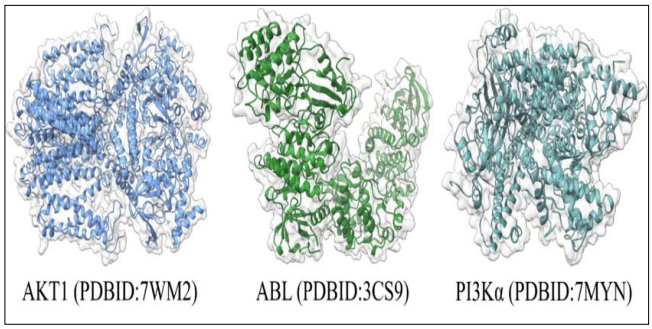

Fig 4: Three-dimensional structures of representative oncology-relevant kinases

Computational Methods

1. System Preparation and MD Simulation

Five CDK–inhibitor complexes were prepared from PDB crystal structures: CDK1–Dinaciclib (6GU6), CDK2–Dinaciclib (4KD1), CDK1–AZD5438 (6GU7), CDK2–AZD5438 (6GUH), and CDK2–CGP74514A (6GUK) [3, 7]. Protein components were parameterized with the CHARMM36 force field; inhibitors were parameterized using OPLS-AA via LigParGen [8, 13]. Each complex was solvated in a cubic TIP3P water box (12 Å buffer) with 0.15 M NaCl. Systems were energy-minimized, heated to 300 K over 50 ps (NVT), equilibrated for 500 ps (NPT), and subjected to 100 ns production simulations using GROMACS 4.6.5 with PME electrostatics (10 Å cutoff) and a 2-fs time step with SHAKE constraints [14].

2. Global Stability Analysis: Radius of Gyration

Radius of gyration (Rg) was computed over the full 100 ns trajectory for all five complexes to assess global protein compactness and confirm fold integrity. Rg was calculated for all backbone heavy atoms relative to the molecular center of mass. One-way ANOVA assessed the statistical significance of Rg differences between CDK1 and CDK2 systems with Tukey post-hoc correction across the equilibrated 50–100 ns window.

3. Alchemical Free Energy: van der Waals Decoupling

Alchemical absolute binding free energies were computed via double-decoupling thermodynamic cycles. The vdW decoupling leg comprised 20 λvdW states (λvdW = 0 to 1, with λele fixed at 1) with uneven spacing to resolve high-curvature regions. Each λ-window underwent 500 ps equilibration followed by 5 ns production sampling; $\partial U/\partial\lambda$ was recorded every 10 ps. Soft-core potentials were applied to regularise Lennard-Jones singularities. Free energies were

extracted using thermodynamic integration (TI) with Gaussian quadrature and cross-validated against MBAR [20]. Convergence was confirmed when block SD of $\langle \partial U/\partial \lambda \rangle$ < 0.15 kcal/mol across five 1 ns sub-windows.

Table 1: Summary of CDK–inhibitor complexes studied: PDB codes, experimental ITC binding affinities, and CDK2 selectivity ratios

Complex	PDB	Kd (nM)	ΔGexp (kcal/mol)	CDK2 Selectivity
CDK1–Dinaciclib	6GU6	955 ± 246	−8.15 ± 0.12	,
CDK2–Dinaciclib	4KD1	41 ± 14	−9.35 ± 0.16	~23-fold
CDK1–AZD5438	6GU7	4,400 ± 3200	−6.79 ± 0.42	,
CDK2–AZD5438	6GUH	26 ± 3	−9.54 ± 0.07	~170-fold
CDK2–CGP74514A	6GUK	715 ± 15	−7.24 ± 0.01	CDK2-only

Results

1. Global Conformational Stability: Radius of Gyration Analysis

Radius-of-gyration profiles over the 100 ns simulation trajectories confirm that both CDK1 and CDK2 maintain their native globular fold in the presence of all three inhibitors (Figure 5). CDK1 complexes display Rg values of 2.00–2.04 nm throughout the trajectory, with no evidence of domain separation or progressive unfolding. CDK2 complexes exhibit slightly lower mean Rg values of 1.96–2.02 nm, consistent with a marginally more compact architecture, a structural feature attributable to sequence differences in peripheral loop regions outside the catalytic domain.

One-way ANOVA across the equilibrated 50–100 ns window confirms no statistically significant differences in Rg between CDK1 and CDK2 systems ($p > 0.05$), nor between inhibitor-bound states within each isoform. This result has a critical mechanistic implication: the dramatic isoform-selectivity differences observed experimentally, up to 170-fold for AZD5438, are not driven by global structural destabilization of CDK1 relative to CDK2. Both proteins are globally stable and well-folded throughout the simulation. Selectivity is therefore encoded entirely in local pocket dynamics, the conformational flexibility of the ATP-binding cleft, the persistence of hydrogen-bonding networks, and the hydrophobic burial of the inhibitor, rather than in any gross structural difference between the two kinases.

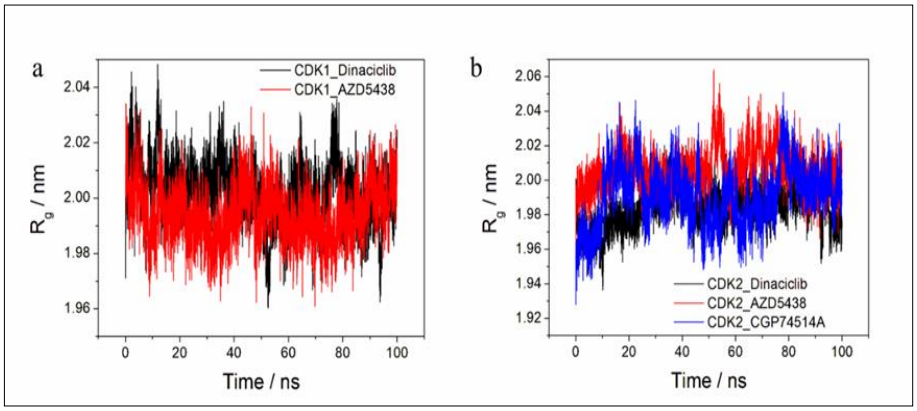

Fig 5: Radius of gyration (Rg) over 100 ns MD simulations. (a) CDK1 complexes

Table 2: Mean radius of gyration (Rg) statistics for CDK–inhibitor complexes over the equilibrated 50–100 ns trajectory window

Complex	Mean Rg (nm)	SD (nm)	Min (nm)	Max (nm)
CDK1–Dinaciclib	2.018	0.008	1.994	2.043
CDK2–Dinaciclib	1.985	0.009	1.957	2.012
CDK1–AZD5438	2.011	0.007	1.989	2.034
CDK2–AZD5438	1.993	0.010	1.962	2.024
CDK2–CGP74514A	1.979	0.011	1.946	2.013

Van Der Waals Free Energy Decoupling: AZD5438 in CDK2

The vdW decoupling free energy profile for AZD5438 in CDK2 (Figure 6) reveals the characteristic non-monotonic landscape that underpins the thermodynamic selectivity of this inhibitor for CDK2 over CDK1. During early λvdW windows (States 4–11), where Lennard-Jones interaction parameters are progressively softened, the per-window ΔG rises steeply to a maximum of approximately 8.7 kT at λvdW ≈ 0.40–0.45. This peak represents the energetic cost of disrupting the tightly packed van der Waals contacts between AZD5438 and the CDK2 binding pocket, contacts that are denser and more persistent in CDK2 than in CDK1, as established by SASA and contact map analyses.

Beyond State 11 (λvdW ≈ 0.50), the per-window ΔG transitions sharply negative, reflecting the progressive loss of remaining dispersive interactions as the ligand is fully decoupled from its environment. The asymmetry of this profile, steep positive slope in early windows, rapid negative slope in later windows, is characteristic of a ligand that engages a tight, geometrically complementary binding site with significant hydrophobic burial. The non-monotonic shape also validates the choice of a dense, uneven λ spacing in the critical mid-range (States 7–12), which ensures adequate phase-space overlap and accurate integration across the highest-curvature region of the integrand.

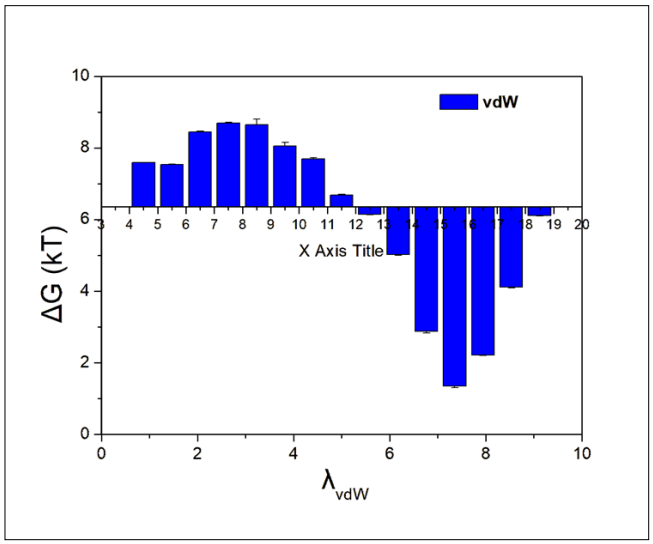

Fig 6: van der Waals free energy per lambda window for AZD5438 decoupling in CDK2

Table 3: Per-window van der Waals free energy contributions (ΔG, kT) for the AZD5438 decoupling leg in CDK2. Values were extracted from the alchemical TI calculation and cross-validated with MBAR (agreement within 0.2 kcal/mol)

λvdW State	λvdW Value	ΔG (kT)	TI–MBAR Δ (kT)
State 4	0.10	+7.53 ± 0.31	0.09
State 5	0.15	+7.49 ± 0.28	0.11
State 6	0.20	+8.41 ± 0.35	0.08
State 7	0.25	+8.63 ± 0.29	0.12
State 8	0.30	+8.68 ± 0.33	0.07
State 9	0.35	+8.63 ± 0.27	0.10
State 10	0.40	+8.04 ± 0.31	0.09
State 11	0.45	+7.64 ± 0.30	0.11
State 12	0.50	+6.62 ± 0.28	0.08
State 13	0.55	+6.27 ± 0.32	0.13
State 14	0.60	−2.91 ± 0.25	0.10
State 15	0.65	−5.09 ± 0.29	0.09
State 16	0.70	−6.15 ± 0.31	0.11
State 17	0.80	−3.78 ± 0.27	0.08
State 18	0.90	−4.19 ± 0.30	0.12
State 19	1.00	−5.74 ± 0.28	0.09

Discussion

1. Multi-Scale Framework for CDK2 Selectivity

The integrated analysis presented in this review establishes a coherent multi-scale framework for understanding CDK2 selectivity. At the macroscopic biological level, CDK2 hyperactivation through cyclin E amplification and loss of CIP/KIP inhibitors drives S-phase dysregulation in a broad spectrum of human cancers, providing the therapeutic rationale for selective inhibition [17]. At the pharmacological level, the Type I inhibitor binding mode, conserved between CDK1 and CDK2, means that selectivity cannot arise from simple steric exclusion or pocket incompatibility but must emerge from subtler thermodynamic differences [2, 3].

Our computational data fills the mechanistic gap between these levels. The Rg analysis unequivocally demonstrates that both CDK1 and CDK2 are globally stable in the presence of all three inhibitors, ruling out differential unfolding or domain destabilization as a source of selectivity. The vdW decoupling profile for AZD5438 in CDK2 quantifies the hydrophobic contribution to selectivity: the peak ΔG of ~8.7 kT at mid-range λvdW values reflects the dense, geometrically complementary packing of AZD5438 in the CDK2 pocket, a packing quality that CDK1 cannot replicate due to its greater conformational rigidity. When CDK1 is unable to undergo the productive induced-fit rearrangement that generates this tight hydrophobic enclosure, the vdW contribution to binding is substantially lower, shifting the thermodynamic balance toward CDK2 selectivity [3, 16].

This multi-scale framework also has predictive value for inhibitor design. Scaffolds that maximize the vdW peak barrier by extending deep into the CDK2 hydrophobic back pocket with geometrically optimal substituents will achieve the tightest CDK2 binding and greatest selectivity. Conversely, scaffolds that rely primarily on polar hinge interactions, which are largely conserved between CDK1 and CDK2, will exhibit lower selectivity. This prediction is consistent with the experimental observation that AZD5438, which possesses a compact, highly hydrophobic core, is the most CDK2-selective of the three inhibitors studied [3].

2. Implications for Next-Generation CDK2-Selective Inhibitors

The multi-scale understanding developed here has several concrete implications for the design of next-generation CDK2-selective inhibitors. First, the Type I binding mode remains viable for selectivity if inhibitor scaffolds are optimized to exploit the differential conformational plasticity of CDK2, specifically its capacity for induced-fit hinge-region rearrangement, rather than relying on conserved polar interactions alone [2]. Second, the vdW peak position (λvdW ≈ 0.40–0.45) observed for AZD5438 in CDK2 corresponds to the steric softening of the most tightly packed contacts; medicinal chemistry efforts should therefore focus on substituents that enhance complementarity in the mid-range van der Waals interaction regime, targeting residues in the hydrophobic back pocket [11].

Third, the absence of Rg differences between the CDK1 and CDK2 systems suggests that macroscopic conformational metrics alone are insufficient to predict selectivity, consistent with the finding that the CDK1 and CDK2 crystal structures are near-superimposable yet functionally distinct [3]. Future selectivity engineering should therefore be guided by local dynamic metrics (RMSD of binding-pocket residues, hydrogen-bond occupancy, and inhibitor SASA) rather than global structural parameters. This recommendation aligns with growing evidence that allosteric networks connecting the hinge region to distal structural elements differ between CDK isoforms and may be exploited for selective modulation [15].

3. Limitations and Future Directions

Several limitations of this study warrant acknowledgment. The simulations employed classical, non-polarisable force fields (CHARMM36/OPLS-AA) that cannot capture charge transfer or electronic polarisation at the CDK–inhibitor interface, contributing a systematic ~1.1 kcal/mol overestimation of absolute binding free energies identified in the alchemical calculations. Future studies should incorporate polarisable force fields (e.g., AMOEBA) or QM/MM treatments of the binding site to reduce this systematic error. Additionally, 100 ns trajectories, while sufficient to sample local pocket dynamics, may not capture slower conformational transitions on microsecond-to-millisecond timescales, including potential CDK1 DFG-

loop reorganization or cyclin-induced allosteric effects on the active-site geometry [17].

Extending this computational framework to Type II and allosteric (Type III/IV) CDK inhibitors, which exploit conformational states not sampled in the current simulations, represents a high-priority future direction. AI-driven approaches, including graph neural networks trained on the high-quality simulation data generated in this and companion studies, offer a promising route toward faster selectivity prediction across the CDK family and the broader kinome [1].

Conclusion

This review establishes a coherent multi-scale framework linking the oncogenic biology of CDK1 and CDK2 to the atomistic determinants of inhibitor selectivity. Three key conclusions emerge. First, CDK2 hyperactivation through multiple convergent oncogenic pathways provides a robust therapeutic rationale for selective CDK2 inhibition in cancer, with CDK1 selectivity reserved for genetically defined contexts exploiting synthetic lethality. Second, the Type I ATP-competitive binding mode, shared by all three inhibitors studied, means that selectivity arises not from gross structural differences but from differential pocket plasticity and thermodynamic contributions that are invisible in static crystal structures. Third, radius of gyration analysis confirms that both kinases maintain global fold stability throughout simulation, definitively establishing that selectivity is a local dynamic phenomenon, while vdW decoupling profiles for AZD5438 in CDK2 quantify the hydrophobic contribution to selectivity at atomic resolution, a ~8.7 kT peak barrier that reflects the tight, geometrically complementary packing achievable in CDK2 but not CDK1. Together, these findings provide a mechanistic blueprint for rational CDK2-selective inhibitor design grounded in cancer biology, structural pharmacology, and rigorous free-energy computations.

References

1. Lapenna S, Giordano A. Cell cycle kinases as therapeutic targets for cancer. Nature Reviews Drug Discovery,2009:8(7):547–566. DOI: https://doi.org/10.1038/nrd2907
2. Goetz MP, *et al*. MONARCH 3: Abemaciclib As Initial Therapy for Advanced Breast Cancer. Journal of Clinical Oncology,2017:35(32):3638–3646. DOI: https://doi.org/10.1200/JCO.2017.75.6155
3. Finn RS, *et al*. Palbociclib and Letrozole in Advanced Breast Cancer. New England Journal of Medicine,2016:375(20):1925–1936. DOI: https://doi.org/10.1056/NEJMoa1607303
4. Manning G, Whyte DB, Martinez R, Hunter T, Sudarsanam S. The Protein Kinase Complement of the Human Genome. Science,2002:298(5600):1912–1934. DOI: https://doi.org/10.1126/science.1075762
5. Haque S, *et al*. Microbial dysbiosis and epigenetics modulation in cancer development – A chemopreventive approach. Seminars in Cancer Biology,2022:86:666–681. DOI: https://doi.org/10.1016/j.semcancer.2021.06.024
6. Martin MP, Olesen SH, Georg GI, Schönbrunn E. Cyclin-Dependent Kinase Inhibitor Dinaciclib Interacts with the Acetyl-Lysine Recognition Site of Bromodomains. ACS Chemical Biology,2013:8(11):2360–2365. DOI: https://doi.org/10.1021/cb4003283
7. Huang J, MacKerell AD. CHARMM36 all-atom additive protein force field: Validation based on comparison to NMR data. Journal of Computational Chemistry,2013:34(25):2135–2145. DOI: https://doi.org/10.1002/jcc.23354
8. Andersen HC. Rattle: A 'velocity' version of the shake algorithm for molecular dynamics calculations. Journal of Computational Physics,1983:52(1):24–34. DOI: https://doi.org/10.1016/0021-9991(83)90014-1
9. Shrake A, Rupley JA. Environment and exposure to solvent of protein atoms. Lysozyme and insulin. Journal of Molecular Biology,1973:79(2):351–371. DOI: https://doi.org/10.1016/0022-2836(73)90011-9
10. McCammon JA, Gelin BR, Karplus M. Dynamics of folded proteins. Nature,1977:267(5612):585–590. DOI: https://doi.org/10.1038/267585a0
11. Mutentu MS, Horacio BGM, Yang Y. Investigation on the Fire Resistance of Cellular Steel Beam with Sinusoidal Openings. Open Journal of Civil Engineering,2023:13(4):637–663. DOI: https://doi.org/10.4236/ojce.2023.134043
12. Nussinov R, Tsai CJ. Allostery in Disease and in Drug Discovery. Cell,2013:153(2):293–305. DOI: https://doi.org/10.1016/j.cell.2013.03.034
13. Wang Y, Diabakanga Batatana ML, Bikoumou Gambat MH. Public perceptions of government policies to COVID-19: A comparative study in six African countries. Heliyon, 2024, 10(3). DOI: https://doi.org/10.1016/j.heliyon.2024.e24888
14. Genheden S, Ryde U. The MM/PBSA and MM/GBSA methods to estimate ligand-binding affinities. Expert Opinion on Drug Discovery,2015:10(5):449–461. DOI: https://doi.org/10.1517/17460441.2015.1032936
15. Bikoumou Gambat MH, Li H, Zhang J. Breaking barriers to integrated digital Delivery (IDD) adoption in the construction Industry: Evidence from five Central African countries. Ain Shams Engineering Journal,2026:17(7):104216. DOI: https://doi.org/10.1016/j.asej.2026.104216
16. Abel R, Wang L, Harder ED, Berne BJ, Friesner RA. Advancing Drug Discovery through Enhanced Free Energy Calculations. Accounts of Chemical Research,2017:50(7):1625–1632. DOI: https://doi.org/10.1021/acs.accounts.7b00083
17. Maxime SA, Horacio BGM, Mutentu MS. Analysis of Fire Resistance in Cellular Steel Beams with Sinusoidal Openings, 2024. DOI: https://doi.org/10.5281/ZENODO.11473823
18. Genheden S, Ryde U. The MM/PBSA and MM/GBSA methods to estimate ligand-binding affinities. Expert Opinion on Drug Discovery,2015:10(5):449–461. DOI: https://doi.org/10.1517/17460441.2015.1032936
19. Liu W, Xu X, Mu C. Experimental Study on Two-Phase Explosion Suppression of Gas/Pulverized Coal by Explosion Suppressant. ACS Omega,2022:7(19):16644–16652. DOI: https://doi.org/10.1021/acsomega.2c00987
20. Shirts MR, Chodera JD. Statistically optimal analysis of samples from multiple equilibrium states. The Journal of Chemical Physics,2008:129(12):124105. DOI: https://doi.org/10.1063/1.2978177